



## Original Article

Simulation and assessment of  $^{99m}\text{Tc}$  absorbed dose into internal organs from cardiac perfusion scan

Saghar Salari, Abdollah Khorshidi\*, Jamshid Soltani-Nabipour

Department of Medical Radiation Engineering, Parand Branch, Islamic Azad University, Parand, Iran

## ARTICLE INFO

## Article history:

Received 3 June 2022

Received in revised form

10 August 2022

Accepted 22 August 2022

Available online 28 August 2022

## Keywords:

Cardiac scan

Internal organ dosage

Radiopharmaceutical technetium

Specific absorbed fraction

Zubal phantom

GATE simulator

## ABSTRACT

Directly, it is not possible to measure the absorbed dose of radiopharmaceuticals in the organs of the human body. Therefore, simulation methods are utilized to estimate the dose in distinct organs. In this study, individual organs were separately considered as the source organ or target organ to calculate the mean absorption dose, which SAF and S factors were then calculated according to the target uptake via MIRD method. Here,  $^{99m}\text{Tc}$  activity distribution within the target was analyzed using the definition and simulation of ideal organs by summing the fraction of cumulative activities of the heart as source organ. Thus, GATE code was utilized to simulate the Zubal humanoid phantom. To validate the outcomes in comparison to the similar results reported, the accumulation of activity in the main organs of the body was calculated at the moment of injection and cardiac rest condition after 60 min of injection. The results showed the highest dose absorbed into pancreas was about 21%, then gallbladder 18%, kidney 16%, spleen 15%, heart 8%, liver 8%, thyroid 7%, lungs 5% and brain 2%, respectively, after 1 h of injection. This distinct simulation model may also be used for different periods after injection and modifying the prescribed dose.

© 2022 Korean Nuclear Society, Published by Elsevier Korea LLC. This is an open access article under the CC BY-NC-ND license (<http://creativecommons.org/licenses/by-nc-nd/4.0/>).

## 1. Introduction

Nuclear medicine is a branch of medicine and molecular radiography that uses the nuclear properties of radioisotopes to diagnose and treat diseases. One of the main isotopes widely used in nuclear medicine is technetium-99 m. The use of  $^{99m}\text{Tc}$  allows for higher activities (up to 1110 MBq or 30 mCi) due to its short half-life of 6.02 h as  $^{99m}\text{Tc}$  is quickly cleared from the blood, along with a fine myocardial absorption and a satisfactory myocardial-to-background ratio for myocardial imaging, particularly in coronary artery disease [1–6]. The procedure consists of first labeling the radio-pharmaceutical for each organ with the appropriate chemical ligand and injecting it into the vein in order to accumulate in the target organ of the patient. Also, some procedures use pure  $^{99m}\text{Tc}$  in the form of pertechnetate ( $\text{TcO}_4^-$ ) [7]. Then, the gamma camera is used to map the metabolic distribution and diagnose the dysfunction [8,9]. In contrast to radiological procedures, which usually provide data about the structure of patient organs, nuclear medicine procedures usually give distinct data about the function

of various organs in the patient body [10–13]. Directly, it is not possible to measure the absorbed dose of radiopharmaceuticals in the human body organs. For this reason, simulation methods are utilized to estimate the dose in dissimilar organs. In this research, individual organs are separately considered as the source (source organ or source limb) to estimate the mean absorption dose, which is then calculated according to the target organ by S factor (mean absorbed dose per accumulated activity) and SAF (Specific Absorbed Fraction) parameter through MIRD (Medical Internal Radiation Dose) method (<http://www.nndc.bnl.gov/mird>). Here, the Zubal phantom [14] is simulated via GATE simulator (<http://www.opengatecollaboration.org/>) to calculate the accumulated activity in the source organ and adjacent organs.

## 2. Methods and materials

## 2.1. Internal dosage calculations

The absorbed radiation dose is characterized as the value of energy deposited per unit mass. In order to calculate the absorbed dose, we must first determine the object mass ( $m_t$ ), the activity accumulated in the specified object, in addition the activity in the surrounding areas. The frequency  $n$  and the energy  $E$  of any

\* Corresponding author.

E-mail address: [abkhorshidi@yahoo.com](mailto:abkhorshidi@yahoo.com) (A. Khorshidi).

emission at any given radionuclide nucleus decay must also be known. In addition, a value known as the absorbed fraction  $\phi$  is required, that signifies the energy fraction  $r_s$  emitted from the deposited source at the  $r_T$  target. **Thus**, the presented factors can be merged to form a general equation for estimating the dose absorbed by the activity:

$$D(r_T \leftarrow r_S) = \tilde{A}(r_S) \sum_i \frac{ni E_i \phi_i(r_T \leftarrow r_S)}{m_T}, \quad (1)$$

while  $\tilde{A}(r_S)$  is the total activity accumulated over time (the total number of decay of the integrated nucleus in a given period of time) at the source [15]. This collective equation for estimating the absorbed dose can be streamlined using MIRD method, in which the dose is presented to the target accumulated over all source areas as follows:

$$D(r_T) = \sum_S \tilde{A}(r_S) S(r_T \leftarrow r_S), \quad (2)$$

where the value  $S(r_T \leftarrow r_S)$  represents the average dose absorbed by the target per total activity with the time variable within the source. Equation (2) shows the two main materials of internal dose estimations, that are: a)  $\tilde{A}(r_S)$  total number of decays at any defined source area, b)  $S(r_T \leftarrow r_S)$  radionuclide specific emission data and related adsorbed fractions. The total activity of the variable with time  $\tilde{A}(r_S)$  is often prescribed by the activity and forms the time-integrated activity coefficient (TIAC) to report the calculated dose in units of milli-gray per mega-Becquerel per hour ( $\text{mGy MBq}^{-1} \text{h}^{-1}$ ). TIAC was formerly identified as residence time.

The method for computing mean absorbed dose is voxel-S-value approach so called point kernel method for non-uniform activity or gradient activity distribution:

$$\bar{D}(\text{vox}_k) = \sum_{S=0}^N \tilde{A}(\text{vox}_k) S(r_k \leftarrow r_S) \quad (3)$$

The dose estimations can be executed at different spatial levels via defined target and source areas at the level of the organ or limb, the sub-organ, the voxel, and the cell. Here, the organ structure is utilized to calculate the dose to the entire organ, assuming that the activity is evenly or uniformly distributed over the source organ and the dose is also evenly deposited in the target organ.

Conventionally, the dose calculations are executed at the organ level, in which case the total doses of organ are estimated by S values, which for the reference phantoms provided, the average age and sex of the patients have been determined. To calculate the internal dose as summarized by Equation (2) in two specific complementary steps, first, the integrated activity with time  $\tilde{A}(r_S)$  was determined in each source region. Second, the activity data integrated with time were merged with the physical data  $S(r_T \leftarrow r_S)$ , and then the dose values were estimated.

## 2.2. GATE simulations

To simulate  $^{99\text{m}}\text{Tc}$  source in tissue, GEANT4 Monte Carlo GATE package was used to designate the tomography. Monte Carlo simulations use random numbers and have probability in risk analysis in order to generate a distribution of possible values. Meanwhile, multiple calculations are executed each time utilizing a different set of random values of probability functions [4,16–19]. The speed and accuracy of Monte Carlo simulations depend on the number of uncertainties and the range of input parameters.

In this study, a whole-body phantom (including the trunk and head) was simulated called Zubal [14] which is the result of a

computed tomography of an adult male. The Zubal phantom includes different organs described by different ID numbers and voxel numbers to assess the SAF and S factors. Each voxel of the phantom is a cube measuring 4 mm. A structure is made of  $128 * 128 * 256$  voxels that include the head and body of the phantom surrounded by air. Fig. 1 shows the simulated phantom with relevant organs.

Clinically, up to 30 mCi (1110 MBq) are injected depending on the age and sex of the patient, but on average the activity of about 100  $\mu\text{Ci}$  (3.7 MBq) reaches the heart. In simulations, 100  $\mu\text{Ci}$  of  $^{99\text{m}}\text{Tc}$ -MIBI radionuclide was utilized in uniform distribution to determine the uptake ratio in different tissues for heart rest situation after 60 min of injection. Table 1 demonstrates the calculation of Zubal phantom data for GATE code input besides the activity of the source organs for cardiac perfusion scan. The activity percentages have been tabulated according to the number of voxels in the standard phantom, and since the heart was considered as a radioactive source, the activity per voxel is relatively high. However, compared to the gallbladder and spleen, the heart organ has relatively less amount.

According to Rossetti et al. research [20] for heart source, the appropriate and practical time for imaging is 1 h after injection, so that with increasing the time, only the gallbladder shows the most activity percentage, and these data were used as code input presented in Table 1.

## 3. Results

In the simulations, radiation-sensitive organs were considered as target organs and the values of SAF parameter and S factor derived from technetium gamma radiation were obtained from dedicated heart as source. Fig. 2 shows the activity distribution in heart as organ source besides SAF parameter for other different affected organs. Meanwhile, Table 2 demonstrates the obtained S factor and the relevant number of voxels in simulated Zubal phantom.

Also, Fig. 3 depicts the radioactive particles tracks within the assessment of  $^{99\text{m}}\text{Tc}$  activity distribution inside the heart and the other target organs derived from the simulation.

Since the distribution of activity accumulates in different organs, the SAF and S factors were simulated at rest after 1 h of injection and the factors were estimated in other target organs as shown in Fig. 4. Meanwhile, Table 3 presents absorbed fraction factors in the source and target organs along with the relevant number of voxels after 60 min.

Fig. 4 revealed that the highest SAF amount and, therefore, the highest dose of activity distribution in the phantom is accumulated within the pancreas by about 21% and the lowest within the brain by about 2%.

## 4. Discussion

In this study,  $^{99\text{m}}\text{Tc}$  activity distribution in target organs was simulated derived from the cardiac perfusion scan by Zubal phantom. Therefore, SAF and S factors were estimated exactly after the injection (as heart source) and also 1 h after the injection in a relaxed state of the heart. The results demonstrated that the SAF and S factors decreased from the moment of injection by 0.147365 and  $3.30\text{E}-6$  to 1 h after injection by 0.000133 and  $2.98\text{E}-9$ , respectively, with the same number of voxel by 9354. Meanwhile, the highest dose absorbed into the pancreas was estimated about 21%, then gallbladder 18%, kidney 16%, spleen 15%, heart 8%, liver 8%, thyroid 7%, lungs 5% and brain 2%, respectively, from the initial activity. In comparison with Rossetti et al. experiment [20], the accumulated activities over all source areas as absorbed doses were

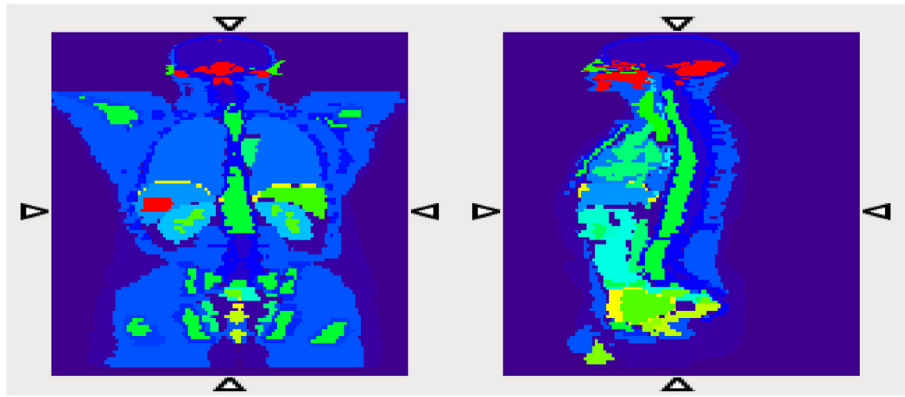


Fig. 1. Standard male Zubal phantom with various texture maps as voxel geometry for GATE code input in coronal (Left) and sagittal (Light) views.

**Table 1**  
Amounts of source-organ activity for GATE code input.

Organs	Activity percentage	Number of voxels	Activity per voxel
<b>Heart</b>	9.1	9345	3.6
<b>Lung</b>	4.4	62374	0.3
<b>Liver</b>	11.4	29277	1.4
<b>Gallbladder</b>	68.6	329	771.7
<b>Spleen</b>	6.4	5568	4.3

in good agreement by maximum  $\pm 2.51$  and minimum  $\pm 0.05$  differences for liver and kidney, respectively. On the other hand, some studies have been performed to determine the ratio of heart to a specific target organ post-injection at rest to evaluate the uptake percentage [2,21,22].

According to  $^{99m}\text{Tc}$  half-life of 6.02 h [23], therefore, the  $\lambda$  decay constant will be  $\ln 2/6.02 = 0.12 \text{ h}^{-1}$ . For example, to calculate the residence time for remaining activity in heart source by 59% as ratio of accumulated activity in heart per administered activity ( $0.1 \text{ mCi} = 3.7 \text{ MBq}$ ), it is  $0.59/0.1/0.12 = 49.2 \text{ h}$ . Meanwhile, accumulated activity per initial activity after injection in target liver by 6% can give the residence time as  $0.06/0.1/0.12 = 5 \text{ h}$ . Therefore, the absorbed dose can be estimated as:  $D = 0.1 \text{ mCi} * 5 \text{ h} * S_{(\text{liver} \leftarrow \text{heart})} = 0.0001 * 3.7 \text{ E}+4 \text{ MBq} * 5 \text{ h} * 3.47\text{E}-7 \text{ mGy/MBq h} = 64.2\text{E}-7 \text{ mGy} = 64.2\text{E}-10 \text{ Gy} = 64.2\text{E}-8 \text{ rad}$ .

On the other hand, in 1 h after injection to estimate the residence time for remaining activity in liver target by 8% as ratio of accumulated activity in liver per administered activity, it will be  $0.08/0.1/0.12 = 6.6 \text{ h}$ . The accumulated activity is determined as the sum of the activity at each moment in time. Then, the absorbed dose can now be estimated as:  $D = 0.1 \text{ mCi} * 6.6 \text{ h} * S_{(\text{liver} \leftarrow \text{heart})}$

**Table 2**  
Derived SAF and S factors (mGy/MBq h) for the heart as source for different organs after injection.

Organ name	ID voxel man	S factor	SAF	No. of voxel
Brain	2	7.98E-09	3.56E-04	18299
Lung	10	6.52E-07	2.91E-02	62374
Heart	11	3.30E-06	0.147365	9354
Liver	12	3.47E-07	0.015496	29277
Gallbladder	13	2.26E-07	0.010072	329
Kidney	14	1.34E-07	0.005962	7618
Pancreas	20	3.97E-07	0.017713	792
Thyroid	28	2.08E-07	0.009285	105
Spleen	31	3.07E-07	0.013726	5568
Urinary bladder	40	1.69E-07	0.004052	3147

$$\leftarrow \text{heart}) = 0.0001 * 3.7 \text{ E}+4 \text{ MBq} * 6.6 \text{ h} * 2.82\text{E}-9 \text{ mGy/MBq h} = 68.9\text{E}-12 \text{ Gy} = 68.9\text{E}-10 \text{ rad}$$

Overall, the reduction dose ratio in liver target after 1 h is calculated by  $64.2 \text{ E}-8/68.9\text{E}-10 = 93.18$ .

The metabolism and pharmacokinetics of radiopharmaceuticals have a major impact on the estimation of the internal absorbed dose. The metabolism like excretions, especially via the liver, urinary bladder, gallbladder or kidneys, also have an influence on the dose received. Experimentally, Boschi et al. [2] have reported different agents of  $^{99m}\text{Tc}$  to evaluate the heart-to-liver ratio for myocardial perfusion imaging so that  $^{99m}\text{Tc}$ -Tetrofosmin (cationic) and  $^{99m}\text{Tc}$ -3SPboroxime (neutral) ligands had the same ratio by 0.8 after 20 min injection. A perfect radio-tracer should have excellent myocardial uptake; a stable and high target to background fraction with low absorption in liver, lungs, stomach and spleen during the imaging; very fast blood clearance and high first pass myocardial

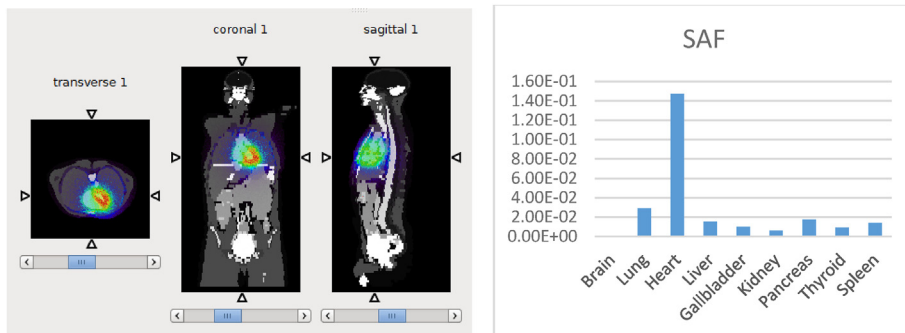


Fig. 2.  $^{99m}\text{Tc}$  activity distribution for heart source simulation (Left) along with obtained SAF parameter to compare with other target organs uptakes after injection (Right).

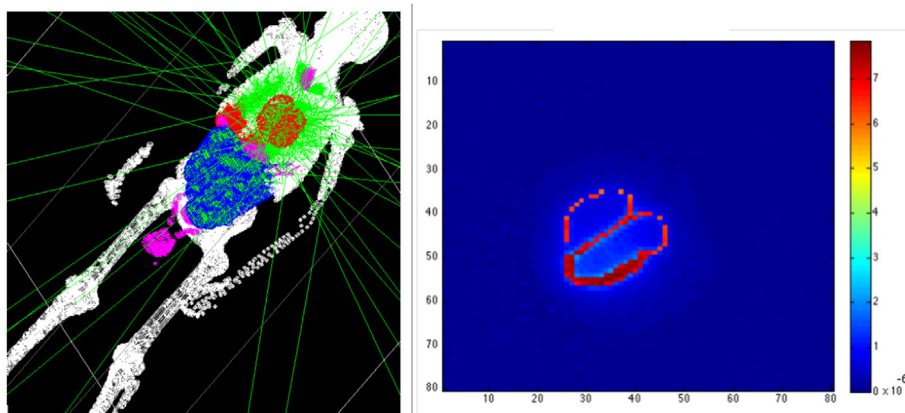


Fig. 3. Particles tracks during activity assessment in heart source and other target organs (Left). Accumulated activity in heart source per administered activity in 1 h after injection (Right).

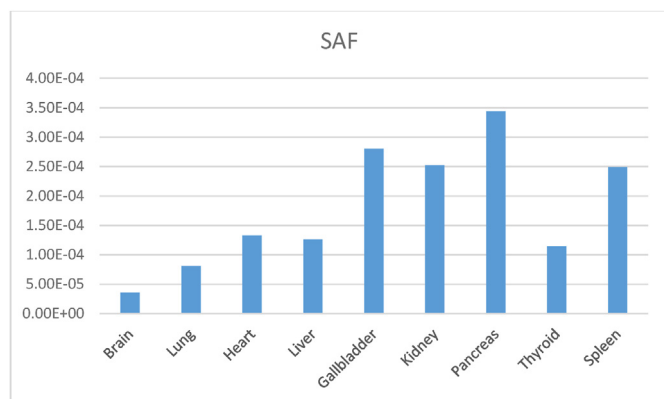


Fig. 4. SAF parameter in heart as source plus target organs at rest condition after 1 h of injection.

Table 3 Estimation of SAF and S factors (mGy/MBq h) besides number of voxels at cardiac rest condition.

Organ name	ID voxel man	S factor	SAF	No. of Vox
Brain	2	7.97E-10	3.56E-05	18299
Lung	10	1.81E-09	8.08E-05	62374
Heart	11	2.98E-09	0.000133	9354
Liver	12	2.82E-09	0.000126	29277
Gallbladder	13	6.26E-09	0.00028	329
Kidney	14	5.65E-09	0.000252	7618
Pancreas	20	7.71E-09	0.000344	792
Thyroid	28	2.56E-09	0.000114	105
Spleen	31	5.59E-09	0.000249	5568
Urinary bladder	40	6.14E-09	0.000339	3147

extraction fraction; and a linear affiliation between coronary blood flow and myocardial uptake of radiotracers [24–26]. Normally, <sup>99m</sup>Tc radioisotope is directly produced by cyclotrons which involves proton bombardment of a solid and fixed <sup>100</sup>Mo target via <sup>100</sup>Mo(p,2n)<sup>99m</sup>Tc reaction. Meanwhile, the indirect production method by cyclotron utilizes <sup>100</sup>Mo(γ,n)<sup>99</sup>Mo and <sup>100</sup>Mo(p,pn)<sup>99</sup>Mo reactions [4]. Alternatively, other production methods are reactor-based routes via low-enrich-Uranium of <sup>235</sup>U(n,fission)<sup>99</sup>Mo and radiative capture by <sup>98</sup>Mo(n,γ)<sup>99</sup>Mo [5,18].

Technetium is a famous transition metal and demonstrates a main disadvantage over other radionuclides when biologically combined with active molecules. For instance, <sup>99m</sup>Tc cannot

alternate for hydrogen or carbon atoms in a target molecule, as is the case with iodine-123 or fluorine-18 or carbon-11 labeling. Imaging with Tc imaging ligands needs deep knowledge on Group 7 metal chemistry besides appropriate ligands designs that yield tough molecular imaging investigations. Familiarity with inorganic chemistry develops expedient pathways to generate stable <sup>99m</sup>Tc into a bio-active molecule with the goal of not influencing its bio-activity. So far, a number of inorganic Tc functional collections that named metal fragments or cores have been introduced to achieve different activity distribution [27]. For example, myocardial uptake of <sup>99m</sup>Tc-Sestamibi is maximal 1 min after injection, and 5 min after injection there is <5% activity within the blood. Therefore, its extraction coefficient by 65% is significantly lower than that of <sup>201</sup>Tl that has the highest cardiac coefficient by 85% between the two blood flow markers of Sestamibi and Tetrofosmin ligands. One hour after the intravenous injection, the cardiac uptake is 1% of the initial injected dose after rest and 1.4% after stress injections, correspondingly. The Sestamibi marker speedily clears from the blood pool and from the hepatobiliary system [1]. On the other hand, Tetrofosmin marker is related to the electronegative trans-membrane possible from the blood to the mitochondrial matrix and, therefore, Tetrofosmin redistribution is negligible and intracellular passage is permanent [28]. Consequently, separate stress and rest imaging are necessary for discerning reversible exercise-related perfusion disorders. The swift clearing by the hepatobiliary system diminishes the main disadvantage of technetium ligands and provides efficient cardiac imaging in addition to reducing and controlling post-injection time.

Dosimetry of smaller limb components that may occur in organs where radiopharmaceutical activity is non-evenly distributed, for instance, a multi-regional kidney sample model can be utilized to execute sub-limb dosimetry [29]. Also, the voxel dose distribution may be calculated derived from the non-uniform activity distribution in the voxels of each dimension. Usually, the voxel dimensions correspond to the voxel size of the SPECT image that is the minimum scale and can be utilized for quantifying the activity in vivo. On the other hand, cell-level dosimetry can be examined using auto-radiographic techniques [24,30,31] or cell dosimetry models [32,33].

### 5. Conclusion

The Zubal phantom with different organs was simulated by GATE code to estimate the affected organs via heart source radiation of <sup>99m</sup>Tc. In simulating cardiac perfusion imaging, MIRD

method was used to calculate SAF and S factors derived from heart on other target organs. Pancreas and brain absorbed, respectively, the maximum and minimum dose by 21% and 2%. In this study, the results of the GATE simulation by maximum 1.5% relative statistical error agreed well with the results of the published articles, and the model at rest may also be utilized for dosimetry during stress, at different times after injection, and for changing the prescribed dose.

### Compliance with ethical standards

Conflict of interest statement: The authors state that there is no conflict of interest.

### Author disclosures

‘The authors have declared no conflicts of interest’.

### Ethical approval

“Not required”.

### Data availability

All data required to support the results and conclusions of the study have been provided here with the submission.

### Declaration of competing interest

The authors declare that they have no known competing financial interests or personal relationships that could have appeared to influence the work reported in this paper.

### References

- [1] F.J.T. Wackers, D.S. Berman, J. Maddahi, D.D. Watson, G.A. Beller, H.W. Strauss, C.A. Boucher, M. Picard, B.L. Holman, R. Fridrich, et al., Technetium-99m hexakis 2-methoxyisobutyl isonitrite: human biodistribution, dosimetry, safety, and preliminary comparison to thallium-201 for myocardial perfusion imaging, *J. Nucl. Med.* 30 (1989) 301–311.
- [2] A. Boschi, L. Uccelli, L. Marvelli, C. Cittanti, M. Giganti, P. Martini, Technetium-99m radiopharmaceuticals for ideal myocardial perfusion imaging: lost and found opportunities, *Molecules* 27 (2022) 1188, <https://doi.org/10.3390/molecules27041188>.
- [3] H. Ma, S. Li, Z. Wu, J. Liu, H. Liu, X. Guo, Comparison of 99mTc-N-DBODC5 and 99mTc-MIBI of myocardial perfusion imaging for diagnosis of coronary artery disease, *BioMed Res. Int.* 2013 (2013) 1–10, <https://doi.org/10.1155/2013/145427>, 145427.
- [4] A. Khorshidi, Accelerator-based methods in radio-material 99Mo/99mTc production alternatives by Monte Carlo method: the scientific-expedient considerations in nuclear medicine, *J. Multiscale Model.* 11 (1) (2020), 1930001, <https://doi.org/10.1142/S1756973719300016>.
- [5] A. Khorshidi, Radiochemical parameters of molybdenum-99 transmutation in cyclotron-based production method using a neutron activator design for nuclear-medicine aims, *Eur Phys J Plus* 134 (2019) 249, <https://doi.org/10.1140/epjp/i2019-12568-3>.
- [6] A. Khorshidi, Neutron activator design for 99Mo production yield estimation via lead and water moderators in transmutation's analysis, *Instrum. Exp. Tech.* 61 (2) (2018) 198–204, <https://doi.org/10.1134/s002044121802015x>.
- [7] G.A. Shabani, F.H. Abbasi, M. Farahani, M. Godarzi, H.R. Khosrounejad, Formulation and quality control of single dose 99mTc-sestamibi as A myocardial perfusion imaging agent, *Iranian J. Nucl. Med.* 18 (1) (2010) 17.
- [8] A. Khorshidi, Assessment of SPECT images using UHRFB and other low-energy collimators in brain study by Hoffman phantom and manufactured defects, *Eur. Phys. J. Plus* 135 (2020) 261, <https://doi.org/10.1140/epjp/s13360-020-00238-6>.
- [9] A. Asgari, M. Ashoor, L. Sarkhosh, A. Khorshidi, P. Shokrani, Determination of gamma camera's calibration factors for quantitation of diagnostic radionuclides in simultaneous scattering and attenuation correction, *Curr. Radiopharmaceut.* 12 (1) (2019) 29–39, <https://doi.org/10.2174/1874471011666180914095222>.
- [10] J.S. Nabipour, A. Khorshidi, Spectroscopy and optimizing semiconductor detector data under X and  $\gamma$  photons using image processing technique, *J. Med. Imag. Radiat. Sci.* 49 (2) (2018) 194–200, <https://doi.org/10.1016/j.jmir.2018.01.004>.
- [11] A. Khorshidi, B. Khosrowpour, S.H. Hosseini, Determination of defect depth in industrial radiography imaging using MCNP code and SuperMC software, *Nucl. Eng. Technol.* 52 (7) (2020) 1597–1601, <https://doi.org/10.1016/j.net.2019.12.010>.
- [12] N. Banihashemi, J. Soltani-Nabipour, A. Khorshidi, H. Mohammadi, Quality control assessment of philips digital radiography and comparison with spellman and samsung systems in tehran oil ministry hospital, *Eur. Phys. J. Plus* 135 (2020) 269, <https://doi.org/10.1140/epjp/s13360-020-00275-1>.
- [13] M. Ashoor, A. Khorshidi, Point-spread-function enhancement via designing new configuration of collimator in nuclear medicine, *Radiat. Phys. Chem.* 190 (2022), 109783, <https://doi.org/10.1016/j.radphyschem.2021.109783>.
- [14] I.G. Zubal, C.R. Harrell, E.O. Smith, Z. Rattner, G. Gindi, P.B. Hoffer, Computerized three-dimensional segmented human anatomy, *Med. Phys.* 21 (1994) 299–302.
- [15] W.E. Bolch, K.F. Eckerman, G. Sgouros, S.R. Thomas, MIRD pamphlet No. 21: a generalized schema for radiopharmaceutical dosimetry—standardization of nomenclature, *J Nucl Med* 50 (3) (2009) 477–484, <https://doi.org/10.2967/jnumed.108.056036>.
- [16] M. Ashoor, A. Khorshidi, Assessment of absorbed dose in deformed breast tissue by Monte Carlo simulation, *SN Appl. Sci.* 2 (2020) 1317, <https://doi.org/10.1007/s42452-020-3113-5>.
- [17] M. Ashoor, A. Khorshidi, Evaluation of crystals' morphology on detection efficiency using modern classification criterion and Monte Carlo method in nuclear, *Proc. of the Nat. Acad. Sci. India Section A - Phys. Sci.* 89 (3) (2019) 579–585, <https://doi.org/10.1007/s40010-018-0482-x>.
- [18] A. Khorshidi, Molybdenum-99 production via lead and bismuth moderators and milli-structure-98Mo samples by the indirect production technique using the Monte Carlo method, *Phys. Uspekhi* 62 (9) (2019) 931–940, <https://doi.org/10.3367/UFNr.2018.09.038441>.
- [19] A. Khorshidi, Accelerator driven neutron source design via beryllium target and 208Pb moderator for boron neutron capture therapy in alternative treatment strategy by Monte Carlo method, *J. Cancer Res. Therapeut.* 13 (3) (2017) 456–465, <https://doi.org/10.4103/0973-1482.179180>.
- [20] C. Rossetti, G. Vanoli, G. Paganelli, M. Kwiatkowski, F. Zito, F. Colombo, C. Bonino, A. Carpinelli, R. Casati, K. Deutsch, M. Marmion, S.R. Woulfe, F. Lunghi, E. Deutsch, F. Ferruccio Fazio, Human biodistribution, dosimetry and clinical use of technetium(III)-99m-Q12, *J. Nucl. Med.* 35 (10) (1994) 1571–1580.
- [21] M. Ghaly, Y. Du, G.S.K. Fung, B.M.W. Tsui, J.M. Links, E. Frey, Design of a digital phantom population for myocardial perfusion SPECT imaging research, *Physics in Medicine and Biology* 59 (2014) 2935–2953, <https://doi.org/10.1088/0031-9155/59/12/2935>.
- [22] L. Volokh, C. Lahat, E. Binyamin, I. Blevis, Myocardial perfusion imaging with an ultra-fast cardiac SPECT camera - a phantom study, *IEEE Nucl. Sci. Sympos. Conf. Record* (2008) 4636–4639.
- [23] A. Khorshidi, M. Sadeghi, A. Pazirandeh, C. Tenreiro, Y. Kadi, Radioanalytical prediction of radiative capture in 99Mo production via transmutation adiabatic resonance crossing by cyclotron, *J. Radioanal. Nucl. Chem.* 299 (2014) 303–310, <https://doi.org/10.1007/s10967-013-2749-7>.
- [24] A. Khorshidi, M. Ahmadinejad, S.H. Hosseini, Evaluation of a proposed biodegradable 188Re source for brachytherapy application: a review of dosimetric parameters, *Medicine* 94 (28) (2015), e1098, <https://doi.org/10.1097/md.0000000000001098>.
- [25] M. Ashoor, A. Khorshidi, A. Pirouzi, A. Abdollahi, M. Mohsenzadeh, S.M.Z. Barzi, Estimation of Reynolds number on microvasculature capillary bed using diffusion and perfusion MRI: the theoretical and experimental investigations, *Eur. Phys. J. Plus* 136 (2021) 152, <https://doi.org/10.1140/epjp/s13360-021-01145-0>.
- [26] M. Ashoor, A. Khorshidi, L. Sarkhosh, Estimation of microvascular capillary physical parameters using MRI assuming a pseudo liquid drop as model of fluid exchange on the cellular level, *Rep. Pract. Oncol. Radiother.* 24 (1) (2019) 3–11, <https://doi.org/10.1016/j.rpor.2018.09.007>.
- [27] A. Boschi, L. Uccelli, P. Martini, A picture of modern Tc-99m radiopharmaceuticals: production, chemistry, and applications in molecular imaging, *Appl. Sci.* 9 (2019) 2526, <https://doi.org/10.3390/app9122526>.
- [28] M. Spadafora, A. Cuocolo, R. Golia, M.L. de Riminil, G. Rosato, V. Rizzo, P. Sullo, L. Florimonte, L. Mansi, P. Miletto, Effect of trimetazidine on 99Tcm-tetrofosmin uptake in patients with coronary artery disease, *Nucl. Med. Commun.* 21 (2000) 49–54.
- [29] L.G. Bouchet, W.E. Bolch, H.P. Blanco, B.W. Wessels, J.A. Siegel, D.A. Rajon, I. Clairand, G. Sgouros, MIRD Pamphlet No 19: absorbed fractions and radionuclide S values for six age-dependent multiregion models of the kidney, *J. Nucl. Med.* 44 (7) (2003) 1113–1147.
- [30] M. Faraggi, I. Gardin, J.L. Stievenart, B.D. Bok, D. Le Guludec, Comparison of cellular and conventional dosimetry in assessing self-dose and cross-dose delivered to the cell nucleus by electron emissions of 99mTC, 123I, 111In, 67Ga and 201Tl, *Eur. J. Nucl. Med.* 25 (3) (1998) 205–214, <https://doi.org/10.1007/s002590050218>.
- [31] A. Khorshidi, A. Rajaei, M. Ahmadinejad, M. Ghoranneviss, M. Ettelaee, Low energy electron generator design and depth dose prediction for micro-

- superficies tumors treatment purposes, *Physica Scripta* 89 (2014), 095001, <https://doi.org/10.1088/0031-8949/89/9/095001>.
- [32] H. Imani-Shirvanehdeh, A. Khorshidi, J. Soltani-Nabipour, A. Alipour, K. Arbabi, Design and construction of a cylindrical ionization chamber for reference dosimetry in radiation protection, *Iran J. Sci. Technol. Trans. Sci.* 45 (2021) 1837–1841, <https://doi.org/10.1007/s40995-021-01153-w>.
- [33] A. Khorshidi, Gold nanoparticles production using reactor and cyclotron based methods in assessment of  $^{196,198}\text{Au}$  production yields by  $^{197}\text{Au}$  neutron absorption for therapeutic purposes, *Mater. Sci. Eng. C* 68 (2016) 449–454, <https://doi.org/10.1016/j.msec.2016.06.018>.